International Journal of Thermal Sciences 48 (2009) 2025–2035

Contents lists available at ScienceDirect

International Journal of Thermal Sciences

journal homepage: www.elsevier.com/locate/ijts

# Contribution of thin-film evaporation during flow boiling inside microchannels

A. Mukherjee*

*Michigan Technological University, 1400 Townsend Drive, Houghton, MI 49931, USA*

ARTICLE INFO

*Article history:*
Received 20 August 2008
Received in revised form
5 March 2009
Accepted 7 March 2009
Available online 22 April 2009

*Keywords:*
Bubble
Flow boiling
Thin-film evaporation

ABSTRACT

Flow boiling through microchannels is characterized by nucleation and growth of vapor bubbles that fill the entire channel cross-sectional area. As the bubbles nucleate and grow inside the microchannel, a thin film of liquid or a microlayer gets trapped between the bubbles and the channel walls. The heat transfer mechanism present at the channel walls during flow boiling is studied numerically. It is then compared to the heat transfer mechanisms present during nucleate pool boiling and in a moving evaporating meniscus. Increasing contact angle improved wall heat transfer in case of nucleate boiling and moving evaporating meniscus but not in the case of flow boiling inside a microchannel. It is shown that the thermal and the flow fields present inside the microchannel around a bubble are fundamentally different as compared to nucleate pool boiling or in a moving evaporating meniscus. It is explained why thin-film evaporation is the dominant heat transfer mechanism and is responsible for creating an apparent nucleate boiling effect inside a microchannel.



## 1. Introduction

Flow boiling inside microchannels is an important area of research as it is capable of removing large amount of heat over small areas. Flow boiling through microchannels is fundamentally different from flow boiling in large diameter channels. In microchannels, bubbles get confined by the channel walls and hence the channel geometry plays an important role in the bubble growth process. At the same time, since the bubbles occupy the entire cross-section of the channels, they regulate the liquid flow as well as the wall heat transfer mechanisms.

It has been observed through several experimental studies that the average wall heat transfer coefficient is dependant on the wall heat flux but is independent of the mass flow rate in the microchannels. That led many researchers to conclude that the heat transfer process is dominated by nucleate boiling mechanisms as opposed to flow boiling mechanisms. Apparently, this seems to be correct reasoning since the growth of individual bubbles confined by the channel walls controls both the thermal and the flow fields inside the microchannels.

It has been long known that a large amount of heat transfer takes place near the contact region of a bubble and a heated wall. A thin layer of liquid, commonly known as the 'microlayer', is believed to be present between a bubble and the wall during the boiling process. In case of boiling process inside a microchannel, the definition of a microlayer becomes ambiguous and many researchers refer to the thin layer of liquid between the bubble and the channel walls as a 'thin-film'.

A large number of analytical and experimental studies have been carried out to quantify the effect of microlayer evaporation on bubble growth in the macro-scale. However, in case of flow boiling inside microchannels, very little work has been reported that quantifies the effect of thin-film evaporation on the bubble growth and the corresponding wall heat transfer. This is mainly due to the limitations of carrying out accurate experiments in the microscale that involves very small length and time scales. Thus, for flow boiling inside microchannels complete numerical solution is necessary to accurately predict the temperature and velocity fields around the growing bubbles and ascertain the effect of thin-film evaporation on the bubble growth.

## 2. Background

### 2.1. Microlayer evaporation

Fig. 1 shows the details of an extended evaporating meniscus on a heated surface. Three regions have been identified here – 1) *Non-evaporating Adsorbed Thin-film Region* – in this region, the liquid is adsorbed on the heater surface and forms a non-evaporating layer. The molecular forces have controlling influence and the disjoining pressure reduces the pressure in the liquid and enables it to reside in a supersaturated liquid state. 2) *Evaporating Thin-film Region* – evaporation occurs at the liquid–vapor interface and liquid is fed

* Tel.: +1 906 487 1174; fax: +1 906 487 2822.
*E-mail address:* mukherje@mtu.edu

1290-0729/$ – see front matter © 2009 Elsevier Masson SAS. All rights reserved.
doi:10.1016/j.ijthermalsci.2009.03.006

**Nomenclature**

| | |
|---|---|
| $A$ | wall area |
| ACA | advancing contact angle |
| $C_p$ | specific heat at constant pressure |
| CA | contact angle |
| $d$ | grid spacing |
| $g$ | gravity vector |
| $H$ | Heaviside function |
| $h$ | heat transfer coefficient |
| $h_{fg}$ | latent heat of evaporation |
| $k$ | thermal conductivity |
| $l_0$ | length scale |
| $m$ | mass transfer rate at interface |
| ms | milliseconds |
| $Nu$ | Nusselt number |
| $p$ | pressure |
| RCA | receding contact angle |
| $Re$ | Reynolds number |
| SH | superheat |
| $T$ | temperature |
| $\Delta T$ | temperature difference, $T_w - T_{sat}$ |
| WV | wall velocity |
| $t$ | time |
| $t_0$ | time scale |
| $u$ | $x$-direction velocity |
| $u_0$ | velocity scale |
| $v$ | $y$-direction velocity |
| $w$ | $z$-direction velocity |
| $x$ | distance in $x$-direction |
| $y$ | distance in $y$-direction |
| $z$ | distance in $z$-direction |
| $\beta_T$ | coefficient of thermal expansion |
| $\kappa$ | interfacial curvature |
| $\mu$ | dynamic viscosity |
| $\nu$ | kinematic viscosity |
| $\rho$ | density |
| $\sigma$ | surface tension |
| $\tau$ | time period |
| $\phi$ | level-set function |
| $\varphi$ | contact angle |

*Subscripts*

| | |
|---|---|
| evp | evaporation |
| in | inlet |
| l | liquid |
| sat | saturation |
| v | vapor |
| w | wall |
| $x$ | $\partial/\partial x$ |
| $y$ | $\partial/\partial y$ |
| $z$ | $\partial/\partial z$ |

*Superscripts*

| | |
|---|---|
| * | non-dimensional quantity |
| → | vector quantity |

from the bulk liquid through the intrinsic meniscus region. Here both the disjoining pressure and the capillary forces play a role. This region is often referred to as the 'microlayer'. 3) *Intrinsic Meniscus Region* – the fluid mechanics in this region is governed by the conventional equation of capillarity.

Derjaguin [1] originally provided the basis of the thin-film evaporation by showing that the net effect, at the macroscopic level, of solid–liquid interactions is a reduction of pressure of the liquid interface relative to the pressure of the equilibrium vapor phase. According to him, the disjoining action could explain the deviation from the laws of hydrostatics that exists in the thin wetting film. Many years later Derjaguin et al. [2] developed an analytical theory and showed that the rate of evaporation from a capillary does not depend on the vapor diffusion through the gas only but also on the transport of liquid through the film caused by the film thickness gradient.

Potash and Wayner [3] studied the transport processes occurring in a two-dimensional evaporating extended meniscus where the fluid flow resulted from both capillarity and disjoining pressure. They calculated the heat flux profile for a given plate superheat and showed that the heat flux reached a maximum in the evaporating thin-film portion of the extended meniscus. Later Wayner and his co-workers [4] analytically calculated the heat transfer coefficient at the interline of an evaporating wetting film.

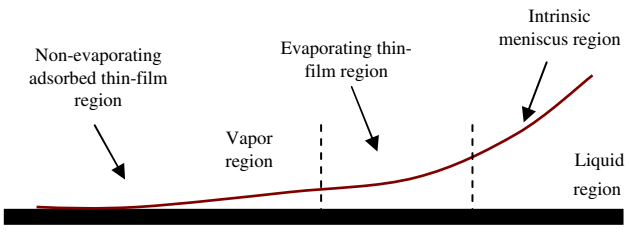


**Fig. 1.** Details of a stationary evaporating meniscus.

Holm and Goplen [5] developed an analytical model to describe heat transfer in capillary grooves. The maximum heat transfer was found to occur in the transition region between the evaporating thin film and the intrinsic meniscus while the evaporating thin-film region was responsible for only eight percent of the total heat transfer.

Sujanani and Wayner [6] measured thicknesses of a completely wetting film on a silicon plate. Their results indicated that the heat transfer and fluid flow phenomena were coupled in the evaporating meniscus. The meniscus was found to oscillate at higher temperature and the oscillations were sensitive to small changes in temperature and pressure. Dasgupta et al. [7] numerically computed thickness profiles of a Heptane meniscus on silicon and compared that with the experimental data. They concluded that significant resistance to heat transfer was present in the contact line region due to conduction, interfacial forces and viscous stresses. In a subsequent work Dasgupta et al. [8] computed the heat flux and the heat transfer coefficients in an evaporating microfilm.

He and Hallinan [9] developed a particle image velocimetry technique to measure the velocity field in an evaporating film. They observed a recirculation zone in the liquid near the contact line region, which they believed to be due to the thermocapillary stresses.

Hoffman and Stephan [10] measured temperatures beneath an evaporating meniscus using thermochromic liquid crystals. A significant temperature drop was observed near the microregion due to presence of a high evaporative heat flux. The wall temperature increased to a higher value in the adsorbed film region due to decreased heat transfer.

Morris [11] analytically calculated heat transfer in an evaporating meniscus of a perfectly wetting fluid. The heat transfer was found to be more in the outer region of the meniscus where the

contact angle and hydrostatic pressure determined the shape of the interface.

### 2.2. Nucleate boiling

A significant amount of literature is available on the effect of microlayer evaporation on vapor bubbles during boiling phenomena and discussion on some of the relevant papers is presented here.

Labunstov [12] identified evaporation near the bubble base as an important mechanism for bubble growth during nucleate boiling. He derived an expression for bubble growth and compared it with the experimental data.

Stephan and Hammer [13] developed an analytical model to study microlayer evaporation during nucleate boiling. They assumed one dimensional heat transfer in the liquid film. The liquid interface temperature was assumed to be greater than saturation temperature due to capillary pressure and the disjoining pressure. One dimensional boundary layer flow was assumed in the film neglecting the convective terms. The microlayer model was coupled with a two-dimensional model of the bubble macroregion. The microregion equations were solved using the Runge Kutta method whereas the macroregion equations were solved using a finite element method. The combined model was solved to study nucleate boiling of refrigerant R-114 on a copper plate. A region of very high heat transfer was noted in the microlayer. The mean heat transfer coefficients obtained from the model agreed reasonably well with the experimental data.

Koffman and Plesset [14] measured microlayer thickness beneath vapor bubbles during nucleate pool boiling using laser interferometry. The fluids used were water and ethanol. Extremely large heat flux of the order of 1000 kW/m$^2$ was observed in the microlayer but it occurred over only very short periods of time and small areas.

Karthikeyan et al. [15] developed an analytical model of a constrained vapor bubble (CVB). They also carried out experiments with a CVB of pentane on a quartz surface and measured the temperature at the intermediate section of the bubble. The analytically obtained profile of the liquid–vapor interface matched well with the experimental data.

Son et al. [16] developed an analytical model of microlayer evaporation present under single vapor bubbles during nucleate pool boiling. They used the lubrication theory to model the fluid flow and heat transfer in the microlayer and added the effect of microlayer evaporation to the macromodel of the vapor bubble. During cyclic growth and departure of the vapor bubbles, the effect of microlayer evaporation to the total wall heat flux was found to be around 20 percent.

### 2.3. Sliding bubbles

It has been experimentally observed that sliding bubbles could significantly enhance wall heat transfer during nucleate boiling. Transient conduction and microlayer evaporation are believed to be primarily responsible for this enhancement in heat transfer.

Sateesh et al. [17] developed an analytical model of sliding bubbles during nucleate pool boiling. The different heat transfer mechanisms such as the microlayer evaporation, transient conduction and the enhanced heat transfer due to sliding bubbles were quantified and compared with the experimental data. The effect of microlayer evaporation was found to be important in the case of organic liquids.

Li et al. [18] made direct measurements of microlayer thicknesses below sliding bubbles in FC-87. They quantified a criterion for development of instabilities in the microlayer based on the shear stress and surface tension forces. The effect of the microlayer evaporation on the bubble dynamics was studied and the microlayer thickness was correlated with the Reynolds number, Weber number and the Froude number.

Recently, Li and Dhir [19] numerically studied bubble dynamics during flow boiling. The effect of microlayer evaporation was included at the bubble base. However, the study did not quantify the effect of microlayer evaporation on the overall wall heat transfer.

### 2.4. Flow boiling in microchannels

Jacobi and Thome [20] hypothesized that thin-film evaporation is the dominant heat transfer mechanism during elongated bubble flow inside microchannels. They developed an analytical heat transfer model consisting of a pair of liquid slug and a vapor bubble. Their model correctly predicted the dependence of convection coefficient on the wall heat flux and liquid mass flux.

Kandlikar [21] identified two new non-dimensional groups K1, K2 relevant to flow boiling inside microchannels. K1 represents the ratio of the evaporation momentum force and the inertia force whereas K2 represents the ratio of the evaporation momentum force and the surface tension force. According to him periodic flow of liquid and vapor slugs resulted in a nucleate boiling mechanism inside the channels diminishing the role of the convective boiling mechanism.

Thome [22] presented a review of flow boiling in microchannels and identified some open issues. He argued that currently there is no definite criterion to identify the threshold between the macro- and the microscale for flow boiling. The author compared different two-phase flow studies conducted by other researchers and showed wide discrepancies in test conditions as well as the results. In the studies that he presented most researchers argued that the heat transfer mechanism is nucleate boiling dominated, as the results show little dependence of the local heat transfer coefficients on the mass velocity. However, since bulk of the heat removal takes place in form of latent heat evaporation, the author contended that thin-film evaporation is the dominant heat transfer mechanism around the elongated bubbles. He supported his case by comparing the results from his two-zone thin-film evaporation model with experimental data.

It is clear from the above literature review that microlayer or thin-film evaporation can play a significant role during the boiling process. However, the contribution of microlayer evaporation can vary significantly depending on the conditions under which the boiling process is taking place. It is a difficult task to accurately ascertain the contribution of microlayer evaporation inside microchannels. A large number of parameters can influence the formation and evaporation of a microlayer that include the flow regimes, thermal boundary conditions, conjugate effects at the walls, dynamic contact angle, channel geometry and the solid, liquid and vapor properties.

## 3. Objective

There are three well known high heat flux applications where evaporation at the three phase contact region plays an important role. These are nucleate pool boiling, a moving evaporating meniscus on a heated surface and flow boiling inside microchannels. However, fundamental physical differences exist between the phenomena of flow boiling inside a microchannel as compared to the other two cases. There is a bulk motion of liquid associated with flow boiling and at the same time the evaporating liquid–vapor interface is confined by the microchannel walls. These factors have significant influence on the shape and motion of the

three phase contact region in case of flow boiling inside a microchannel as compared to the other two cases. In the present study, we compare and contrast the flow and temperature fields near the contact region of the liquid–vapor interface during nucleate pool boiling, evaporation of a moving meniscus and flow boiling inside a microchannel. In all the presented results, the disjoining pressure effect on thin-film evaporation has been ignored. The objective is to qualitatively compare the heat transfer mechanisms in these three cases and ascertain whether thin-film or the microlayer evaporation is the dominant heat transfer mechanism during flow boiling inside a microchannel.

## 4. Numerical method

The following general numerical technique has been used in the flow boiling simulation results presented in this paper.

The complete incompressible Navier–Stokes equations have been solved using the SIMPLER method [23], which stands for Semi-Implicit Method for Pressure-Linked Equations Revised. The continuity equation is turned into an equation for the pressure correction. A pressure field is extracted from the given velocity field. At each iteration, the velocities are corrected using velocity-correction formulas. The computations proceed to convergence via a series of continuity satisfying velocity fields. The algebraic equations are solved using the line-by-line technique, which uses TDMA (Tri-Diagonal Matrix Algorithm) as the basic unit. The speed of convergence of the line-by-line technique is further increased by supplementing it with the block-correction procedure [24]. The multi-grid technique has been employed to solve the pressure equations.

Sussman et al. [25] developed a level-set approach where the interface was captured implicitly as the zero level set of a smooth function. The level-set function was typically a smooth function, denoted as φ. This formulation eliminated the problems of adding/subtracting points to a moving grid and automatically took care of merging and breaking of the interface. Furthermore, the level-set formulation generalized easily to three dimensions. All the numerical analyses presented in this paper have been done using this level-set technique.

The liquid–vapor interface is identified as the zero level set of a smooth distance function φ. The level-set function φ is negative in the vapor zone and positive in the liquid zone. The interface is located by solving the level-set equation. A fifth order WENO (Weighted, Essentially Non-Oscillatory) scheme is used for left sided and right sided discretization of φ [26]. While φ is initially a distance function, it will not remain so after solving the level-set equation. Maintaining φ as a distance function is essential for providing the interface with a width fixed in time. This is achieved by reinitialization of φ. A modification of Godunov's method is used to determine the upwind directions. The reinitialization equation is solved in fictitious time after each fully complete time step. With $\Delta\tau = d/2u_0$, ten $\tau$ steps are taken with a third order TVD (Total Variation Diminishing) Runge Kutta method.

### 4.1. Governing equations

The following equations have been solved during the numerical calculations:

Momentum equation:

$$\rho\left(\frac{\partial \vec{u}}{\partial t} + \vec{u}\cdot\nabla\vec{u}\right) = -\nabla p - \sigma\kappa\nabla H + \nabla\cdot\mu\nabla\vec{u} + \nabla\cdot\mu\nabla\vec{u}^{\mathrm{T}} \tag{1}$$

Energy equation:

$$\begin{aligned} &\rho C_p\left(\tfrac{\partial T}{\partial t} + \vec{u}\cdot\nabla T\right) = \nabla\cdot k\nabla T \ \text{ for } \phi > 0 \\ &T = T_{\mathrm{sat}} \ \text{ for } \phi \le 0 \end{aligned} \tag{2}$$

Continuity equation:

$$\nabla\cdot\vec{u} = \frac{\vec{m}}{\rho^2}\cdot\nabla\rho \tag{3}$$

The curvature of the interface:

$$\kappa(\phi) = \nabla\cdot\left(\frac{\nabla\phi}{|\nabla\phi|}\right) \tag{4}$$

The mass flux of liquid evaporating at the interface:

$$\vec{m} = \frac{k_{\mathrm{l}}\nabla T}{h_{\mathrm{fg}}} \tag{5}$$

The vapor velocity at the interface due to evaporation:

$$\vec{u}_{\mathrm{evp}} = \frac{\vec{m}}{\rho_{\mathrm{v}}} = \frac{k_{\mathrm{l}}\nabla T}{\rho_{\mathrm{v}} h_{\mathrm{fg}}} \tag{6}$$

To prevent instabilities at the interface, the density and viscosity are defined as

$$\rho = \rho_{\mathrm{v}} + (\rho_{\mathrm{l}} - \rho_{\mathrm{v}})H \tag{7}$$

$$\mu = \mu_{\mathrm{v}} + (\mu_{\mathrm{l}} - \mu_{\mathrm{v}})H \tag{8}$$

$H$ is the Heaviside function given by

$$\begin{aligned} &H = 1 \ \text{ if } \phi \ge +1.5d \\ &H = 0 \ \text{ if } \phi \le -1.5d \\ &H = 0.5 + \phi/(3d) + \sin[2\pi\phi/(3d)]/(2\pi) \ \text{ if } |\phi| \le 1.5d \end{aligned} \tag{9}$$

where $d$ is the grid spacing

Since the vapor is assumed to remain at saturation temperature, the thermal conductivity is given by

$$k = k_{\mathrm{l}}H^{-1} \tag{10}$$

The level-set equation is solved as

$$\frac{\partial\phi}{\partial t} + (\vec{u} + \vec{u}_{\mathrm{evp}})\cdot\nabla\phi = 0 \tag{11}$$

After every time step the level-set function $\phi$, is reinitialized as

$$\frac{\partial\phi}{\partial t} = S(\phi_0)\,(1 - |\nabla\phi|)u_0 \tag{12}$$

$$\phi(x,0) = \phi_0(x)$$

$S$ is the sign function which is calculated as

$$S(\phi_0) = \frac{\phi_0}{\sqrt{\phi_0^2 + d^2}} \tag{13}$$

### 4.2. Scaling factors

All the governing equations are made non-dimensional using a length scale and a time scale. For flow boiling calculations, the length scale $l_0$ given by the channel width (in this case same as the channel height) and is equal to 200 μm. Thus, for water at 100 °C, and $Re = 100$, the velocity scale $u_0$ is calculated as 0.146 m/s. The corresponding time scale $t_0$ is 1.373 ms.

The non-dimensional temperature is defined as

$$T^* = \frac{T - T_{sat}}{T_w - T_{sat}} \tag{14}$$

The Nusselt number ($Nu$) is calculated based on the area-averaged heat transfer coefficient ($\bar{h}$) at the wall given by,

$$\bar{h} = \frac{1}{A}\int_0^A h \, dA \tag{15}$$

where $A$ is the wall area.

The wall Nusselt number is defined as,

$$Nu = \frac{\bar{h} l_0}{k_l} \tag{16}$$

The number of computational cells in the flow boiling domain is $320 \times 80 \times 40$, i.e. 80 grids have been used per $0.99 l_0$. The grid size has been chosen from previous work of Mukherjee and Kandlikar [27] to minimize numerical error and optimize the computation time. The time step used varied typically between 1e−4 and 1e−5. Negligible change in the results is observed when calculations are carried out with smaller time steps, which ensured that calculations are time step independent. All physical properties are taken as constant at 100 °C.

## 5. Results

### 5.1. Nucleate boiling mechanism during pool boiling

Fig. 2 shows contact angle variation at the base of a vapor bubble during nucleate pool boiling [28]. As the bubble grows, the bubble base diameter expands initially, then stays constant for a brief period of time and finally contracts as the bubble departs from the surface. The contact angle at the bubble base varies during the bubble growth period, with the advancing contact angle being greater than the receding contact angle. It is believed that a thin layer of liquid present below the bubble results in very high local heat flux at the wall. However, the liquid motion around the base of the bubble due to the expansion and contraction of the bubble base plays a very important role as well in transient conduction from the wall.

The effect of microlayer evaporation is expected to be significant in case of wetting surfaces where the contact angle is relatively low. Thus, if microlayer evaporation is to be the dominant heat transfer mechanism during nucleate pool boiling, boiling on highly wetting surfaces is expected to remove higher heat flux compared to boiling on non-wetting surfaces. However, on the contrary, it has been experimentally observed that for same amount of wall superheat, heat flux increases with increase in the contact angle [29].

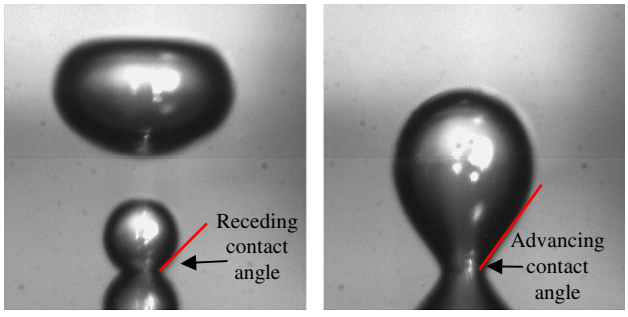


**Fig. 2.** Dynamic contact angle at bubble base during nucleate pool boiling.

Fig. 3 shows the velocity field around a bubble base during nucleate pool boiling [30]. Single vapor bubbles with dynamic contact angle were simulated in that study. The length scale used in the calculations was 2.5 mm and the wall superheat was 10 K. In the first frame of Fig. 3 the advancing contact angle is 54° whereas the receding contact angle is 20°. In the second frame the advancing contact angle is 90° whereas the receding contact angle is 54°. In both the frames the bubble bases are contracting and the bubbles are about to depart at the times shown in the frames. The reference vector has been indicated in both the frames. It is clearly seen that there is an intense liquid circulation present around the bubble base when the contact angle is higher.

Fig. 4 shows the temperature field near the bubble base corresponding to the cases shown in Fig. 3. The thermal boundary layer is thinner at the wall in case of higher contact angle, indicating increased heat transfer from the wall. Table 1 shows the vapor volume growth rates for different values of advancing and receding contact angles used in the calculations. The vapor volume growth rate increases with increase in contact angle which confirms higher rate of heat transfer from the wall. The influence of advancing contact angle on the wall heat transfer is much more pronounced compared to the receding contact angle. The transient conduction mechanism created by the bubble motion plays an important role as the contact angle is increased. When the contact angle decreases, the contribution of microlayer evaporation may increase but at the same time the bubbles become short lived with smaller departure diameters. The larger bubbles are more effective in disturbing the thermal boundary layer formed around the bubbles which results in higher rates of heat transfer.

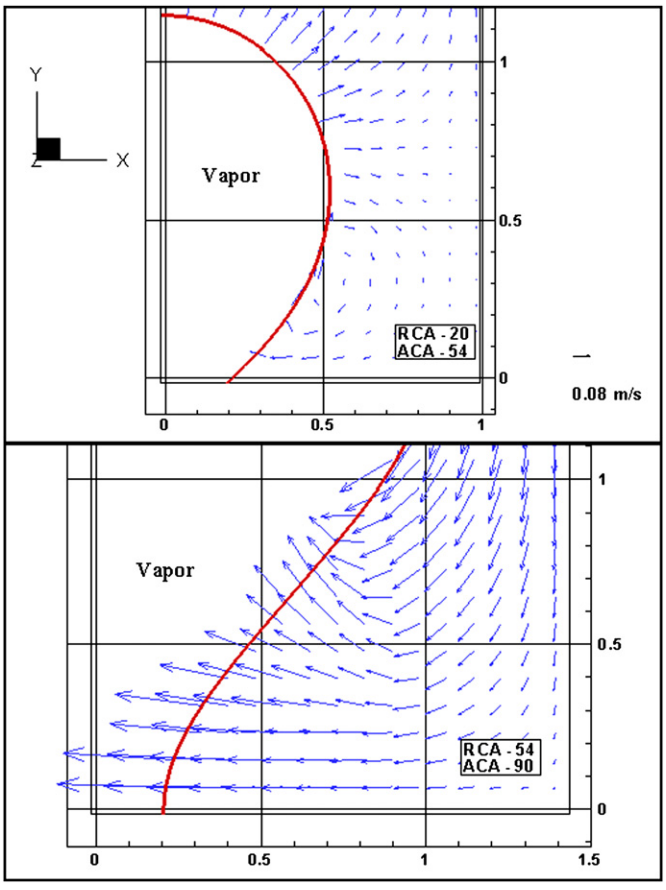


**Fig. 3.** Velocity field in liquid near bubble base during nucleate pool boiling.

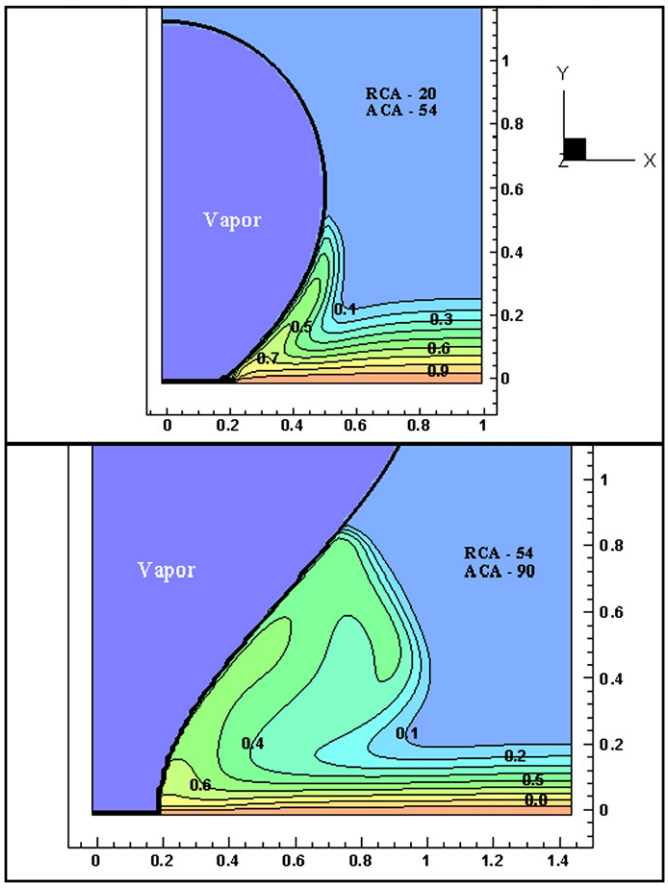


**Fig. 4.** Temperature field near bubble base during nucleate pool boiling.

### 5.2. Transient conduction in a moving and evaporating meniscus

Kandlikar et al. [31] experimentally studied heat transfer from a moving evaporating meniscus. Mukherjee and Kandlikar [32] developed a numerical model of a moving evaporating meniscus on a heated surface and computed the local heat transfer along the base of the meniscus. Fig. 5 shows the numerical model in which the water enters the liquid column from the top and the heated bottom wall moves in the positive *x*-direction. The length scale in this case is 1 mm. Evaporation takes place at both the advancing and receding ends of the meniscus due to heat transfer from the wall into the meniscus.

Fig. 6 shows liquid circulation inside the meniscus due to the motion of the wall. The advancing and receding contact angles in this case are 61° and 48°, respectively. The wall superheat is 5 K and the wall velocity is 0.1 m/s. It is clearly seen that because of the wall motion, the liquid is dragged along the base of the meniscus creating a circulation. Large velocity vectors can be seen along the receding interface of the meniscus in the vapor side, indicating high rates of evaporation along the receding interface. No such intense

**Table 1**
Effect of contact angle on vapor volume growth rates.

| ACA (°) | RCA (°) | Vapor volume growth rate (mm$^3$/ms) |
|---|---|---|
| 61 | 61 | 0.4 |
| 90 | 54 | 0.9 |
| 54 | 20 | 0.3 |

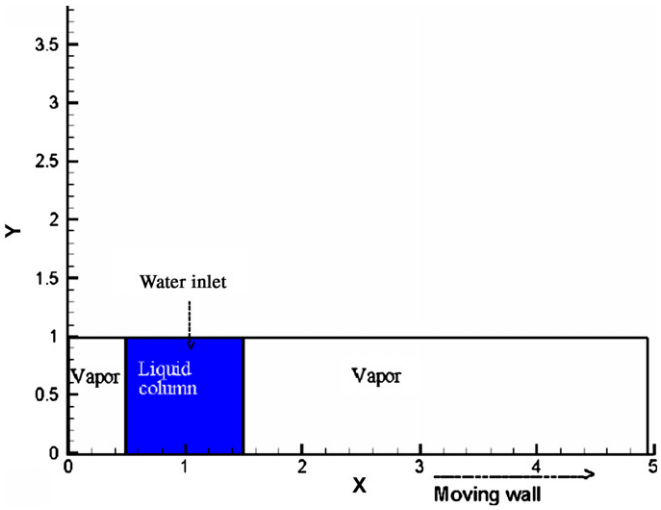


**Fig. 5.** A moving and evaporating meniscus.

evaporation is observed along the advancing interface of the meniscus.

Fig. 7 shows the temperature field inside the meniscus corresponding to the conditions shown in Fig. 6. Isotherms have been plotted for non-dimensional temperature between 0 and 1 at intervals of 0.1. A zone of superheated liquid can be seen along the receding meniscus that causes the intense evaporation which was seen earlier in Fig. 6. The distance between the isotherms along the meniscus base is found to be thicker below the receding interface compared to the advancing interface. This indicates higher rate of heat transfer is occurring at the advancing end of the meniscus base due to transient conduction. The circulation inside the meniscus is bringing the cooler liquid down near the advancing interface while moving the hotter liquid away from the wall along the receding interface.

Fig. 8 compares the variation of the average heat transfer at the meniscus base with time for different values of advancing and receding contact angle. In the first two cases the advancing contact angle was kept constant whereas the receding contact angle was increased. In the last two cases the receding contact angle was kept constant whereas the advancing contact angle was increased. It can

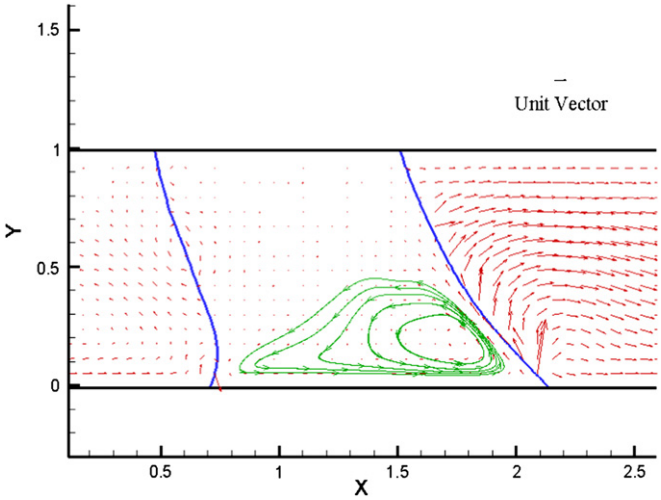


**Fig. 6.** Liquid circulation inside meniscus (ACA – 61°; RCA – 48°; SH – 5 K; WV – 0.1 m/s).

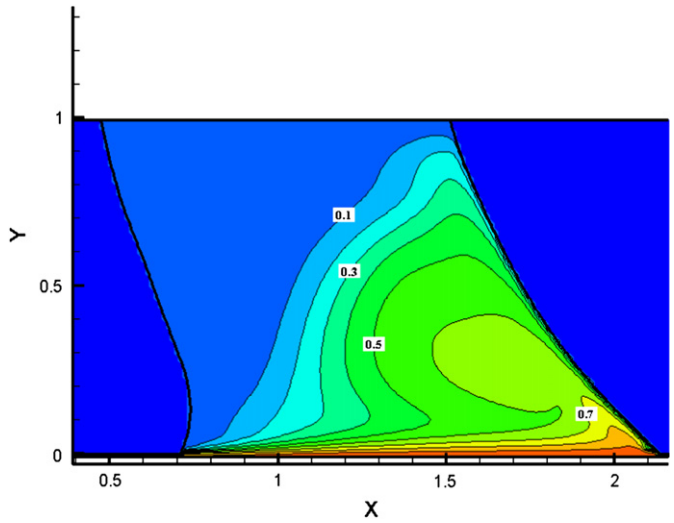


**Fig. 7.** Temperature field inside meniscus (ACA – 61°; RCA – 48°; SH – 5 K; WV – 0.1 m/s).

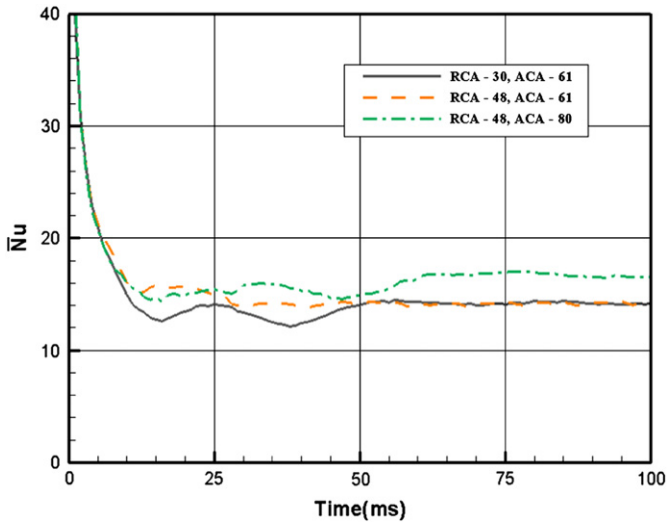


**Fig. 8.** Comparison of average heat transfer coefficient at the meniscus base as a function of contact angle (SH – 5 K; WV – 0.1 m/s).

be clearly seen that overall heat transfer increased with increase in the advancing contact angle only. This indicates the transient conduction present at the advancing contact region is the dominant heat transfer mechanism below the moving evaporating meniscus.

### 5.3. *Effect of contact angle on bubble growth during flow boiling in a microchannel*

Mukherjee and Kandlikar [33] carried out numerical simulation of vapor bubbles with static contact angle during flow boiling inside microchannels. In the present study vapor bubbles are simulated with constant but different values of advancing and receding contact angles. The receding contact angle (RCA) values used are 20°, 40° and 60° and advancing contact angle (ACA) values used are 40°, 60° and 80°. The contact angle is varied linearly between the upstream and the downstream end of the bubble base based on the length of the bubble base. The wall superheat is set to 8 K in all the cases and the length scale is 200 μm.

Fig. 9 shows the bubble shapes for the lowest and highest values of contact angle used in the calculations. The time taken for the bubbles to grow to that size is shown in the bottom corner of each frame. It can be seen that the bubble with lower contact angle has taken less time to grow compared to the bubble with higher contact angle. Both the bubbles show vapor patches on the side walls which indicate reduced heat transfer in the areas where the vapor is in contact with the walls.

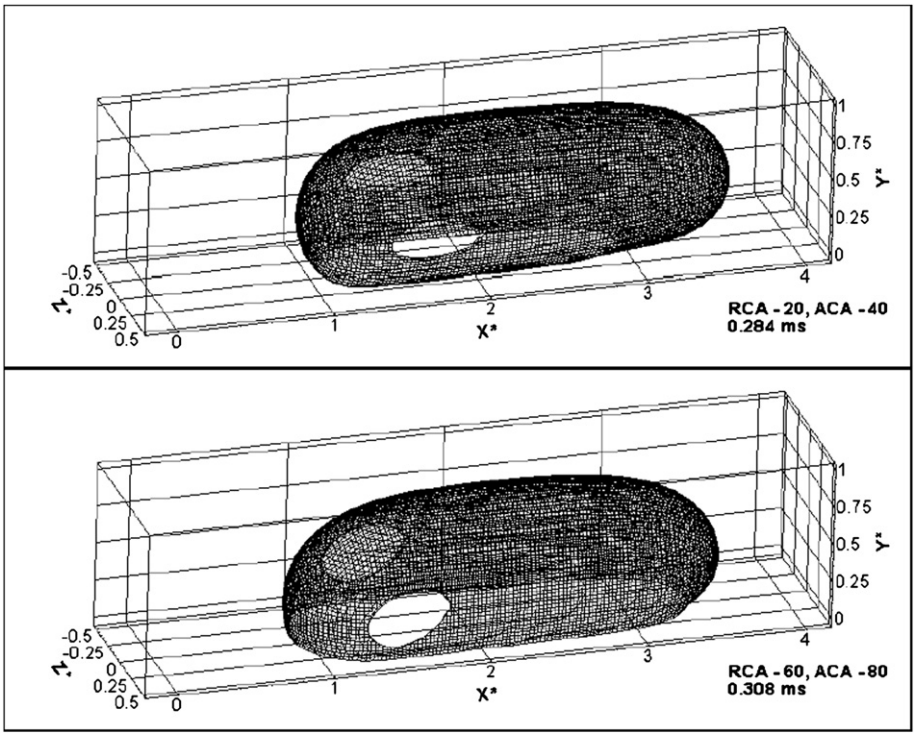


**Fig. 9.** Comparison of bubble shapes with different contact angle.

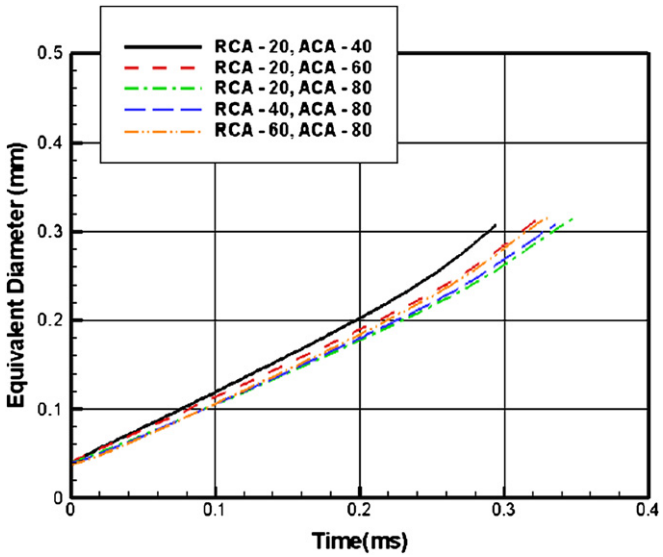


**Fig. 10.** Comparison of bubble equivalent diameters.

Fig. 10 compares the bubble equivalent diameters for the different values of advancing and receding contact angles used in this study. The bubble equivalent diameter is calculated as the diameter of a sphere of equal volume. The bubble with the lowest contact angle used in this study is seen to grow the fastest which indicates higher rate of evaporation around the bubble interface. As the advancing contact angle is increased keeping the receding contact angle at 20° the bubble growth rate is found to decrease. However, when the advancing contact angle is kept constant at 80° and the receding contact angle is increased, the bubble growth rate is seen to improve by a small amount. This is probably due to decrease in the surface tension forces at the receding interface of the bubble base.

Figs. 11 and 12 compare the area-averaged heat transfer at the North and South walls, respectively, as a function of time. North wall is at $y^* = 1$ whereas the South wall is at $y^* = 0$ of the computational domain as seen in Fig. 9. The heat transfer at both the walls is seen to be highest at 0.25 ms for the bubble with the receding contact angle of 20° and advancing contact angle of 40°. The heat transfer at the South wall is found to be lower compared to the North wall as part of the South wall is covered with vapor below the bubble base.

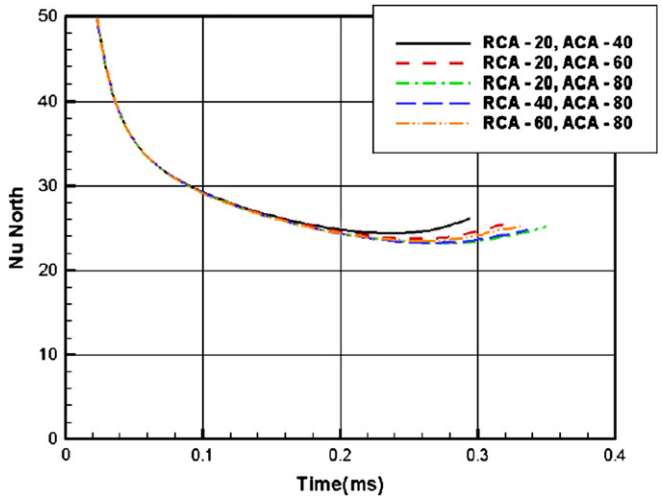


**Fig. 11.** Comparison of heat transfer at the North wall.

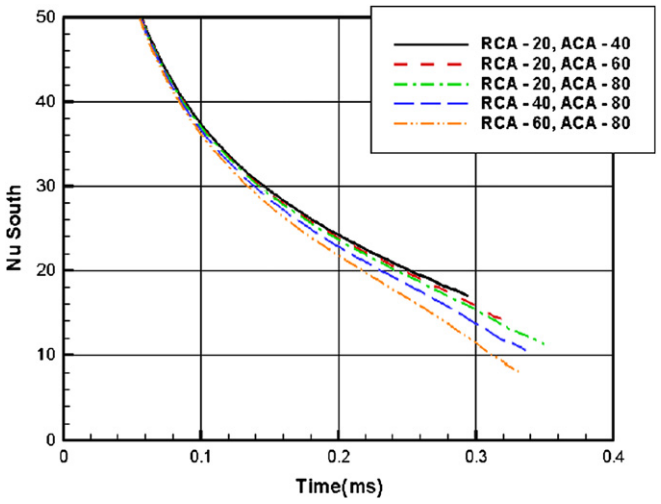


**Fig. 12.** Comparison of wall heat transfer at the South wall.

The heat transfer at the South wall is found to decrease with time since the bubble base length increases due to the bubble growth. At any particular time, the heat transfer at the South wall is found to decrease with increase in both the advancing and the receding contact angles. However, at the North wall the heat transfer improves slightly with increase in receding contact angle for the constant advancing contact angle of 80°. This is due to the slightly higher bubble growth rate which was seen earlier in Fig. 10.

Fig. 13 compares the velocity fields around the bubbles for the lowest and highest contact angle values used in this study. Both frames are at a time of around 0.28 ms after the bubble nucleation. The reference vector has been indicated in each frame. The bubble with the lower contact angle is seen to have grown much bigger comparatively and larger velocity vectors can be seen at the downstream of the bubble. This indicates that this bubble is growing faster compared to the bubble with higher contact angle.

Fig. 14 compares the thermal fields around the bubbles for the cases shown in Fig. 13. In the case of 20° receding contact angle a thin layer of liquid is seen at the receding end below the bubble. The crowding of isotherms in that region indicates a very high rate of local wall heat transfer. The distance between the isotherms at the contact region in the upstream end of the bubble is greater compared to that at the downstream end. This indicates that the heat transfer below the receding interface at the downstream end of the bubble is higher compared to the contact region at the upstream interface.

At the North wall, a thin layer of liquid can be seen between the bubble and the wall in case of the bubble with 20° receding contact angle. This thin layer of liquid evaporates as the bubble grows and results in higher average wall heat transfer at the North wall which was seen earlier in Fig. 11.

## 6. Discussion

It can be argued from the above numerical results that flow boiling inside microchannels involves fundamentally different heat transfer mechanisms as compared to those present during nucleate pool boiling or in an evaporating meniscus on a moving heated surface.

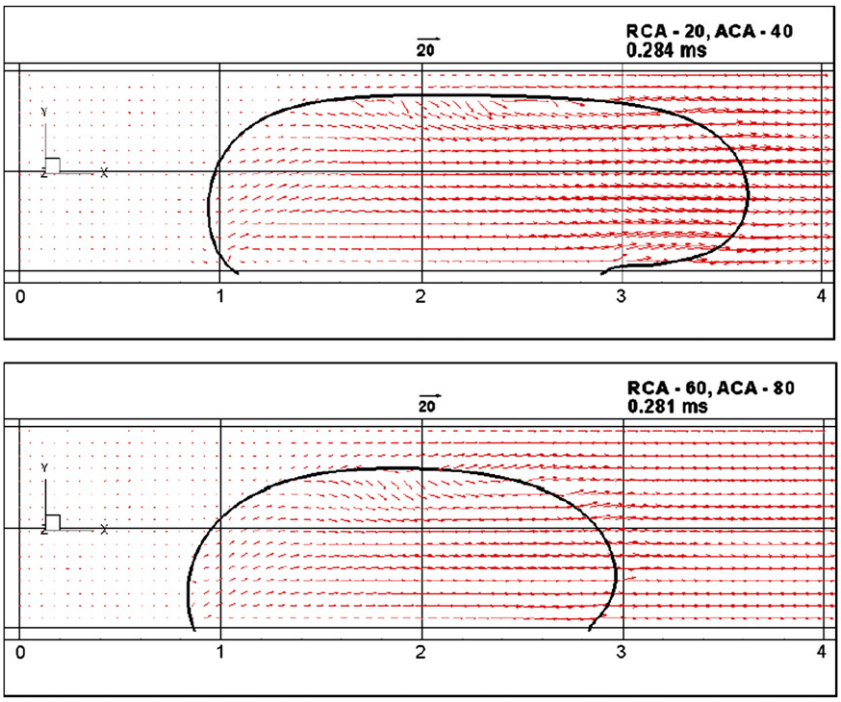


**Fig. 13.** Comparison of velocity fields.

### 6.1. *Effect of change in the contact angle on the wall heat transfer*

In case of nucleate pool boiling and a moving evaporating meniscus, the wall heat transfer was found to increase with increase in the contact angle. However, in case of bubble growth inside microchannels, the wall heat transfer improved with decrease in the contact angle. Since thin-film evaporation is expected to be more effective with decrease in contact angle, this is the first indication that flow boiling inside microchannels is probably dominated by thin-film evaporation.

### 6.2. *Comparison of heat transfer below the advancing and receding interfaces*

We have also seen that heat transfer during nucleate pool boiling improves when the bubble base contracts resulting in

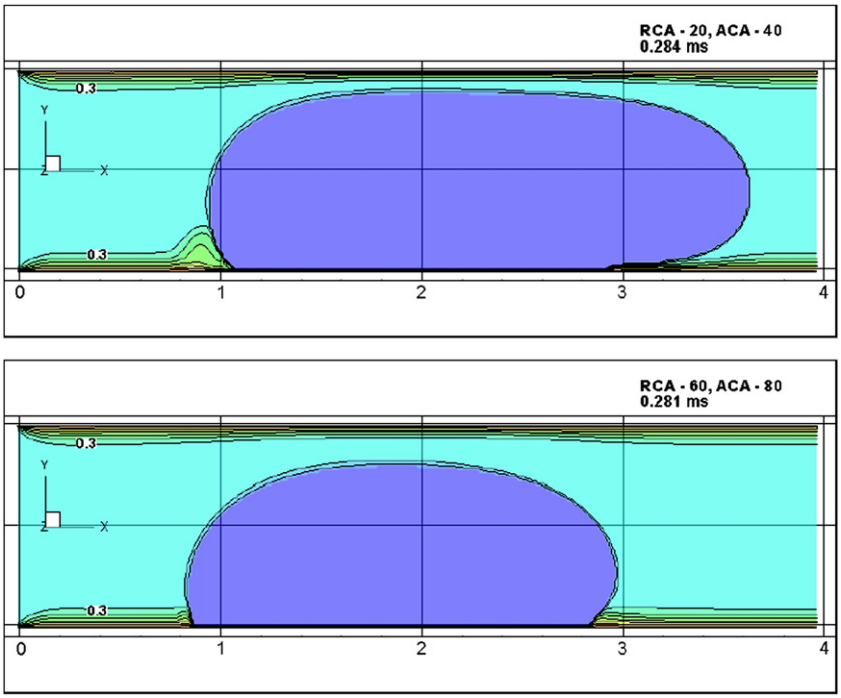


**Fig. 14.** Comparison of temperature fields.

intense liquid circulation around the bubble base. The advancing liquid–vapor interface at the bubble base is primarily responsible for the improved transient conduction at the wall. In case of the moving evaporating meniscus, heat transfer is found to be significantly greater near the advancing interface as compared to the receding interface. However, in the case of the bubble growth inside a microchannel during flow boiling, heat transfer is found to be significantly higher below the receding liquid–vapor interface as compared to the advancing contact region due to the presence of an evaporating liquid layer. This also suggests that the heat transfer mechanism is likely to be dominated by thin-film evaporation in the case of flow boiling inside microchannels.

### 6.3. Absence of liquid circulation

Transient conduction is typically caused by liquid circulation that moves the liquid away from a heated wall and brings cooler liquid towards the wall. In the cases of both nucleate pool boiling and the moving evaporating meniscus, a distinct liquid circulation is observed near the contact line region. However, no liquid circulation is observed during flow boiling inside a microchannel. This observation also hints to the fact that transient conduction may not be a dominant heat transfer mechanism in case of flow boiling inside microchannels.

### 6.4. Impression of nucleate boiling mechanism

In case of flow boiling inside microchannels, the velocities generated by the bubble growth are significantly larger compared to the typical incoming liquid velocities. This is also evident from comparing the velocity vectors at the upstream and downstream ends of the bubble in Fig. 13. The evaporation momentum force at the advancing interface acts in the opposite direction to the incoming liquid and thus the flow and thermal field inside the microchannels are little affected with changes in the incoming liquid mass flux. The bubble growth depends directly on vapor addition from the evaporation of the thin film around it. The rate of this thin-film evaporation increases directly with the wall heat flux. This explains why the wall heat transfer coefficient has been experimentally found to be insensitive to the incoming liquid mass flux but sensitive to the wall heat flux. Thin-film evaporation is primarily responsible for bubble growth inside microchannels during flow boiling but the resultant effect of bubble growth gives rise to an apparent notion of presence of nucleate boiling mechanism.

## 7. Conclusions

The bubble growth during flow boiling inside microchannels is compared to nucleate pool boiling and a moving evaporating meniscus using numerical computations. It is shown that the velocity and thermal fields present around bubbles during flow boiling inside microchannels are fundamentally different than those present around bubbles during nucleate pool boiling or inside a moving evaporating meniscus. During flow boiling inside microchannels, the wall heat transfer is found to improve with decrease in contact angle and is found to be greater below the receding bubble interface compared to the advancing bubble interface. This clearly indicates that thin-film or microlayer evaporation around the bubbles is the primary wall heat transfer mechanism. No liquid circulation is observed inside the microchannel that is often associated with transient heat conduction from a heated surface. It has been explained how thin-film evaporation controls the bubble growth and gives rise to an apparent notion of presence of nucleate boiling mechanism during flow boiling inside a microchannel.

## Acknowledgment

The work was conducted in the Advanced Energy Systems and Microfluidics Laboratory at MTU.

## References

[1] B. Derjaguin, A theory of capillary condensation in the pores of sorbents and of other capillary phenomena taking into account the disjoining action of polymolecular liquid films, Acta Physicochim. U.R.S.S. 12 (2) (1940) 181–200.
[2] B.V. Derjaguin, S.V. Nerpin, N.V. Churaykev, Effect of film transfers upon evaporating liquids, International Association of Testing and Research Laboratories for Materials and Structures 29 (1) (1965) 93–98.
[3] M. Potash Jr., P.C. Wayner Jr., Evaporation from a two-dimensional extended meniscus, Int. J. Heat Mass Transfer 15 (1972) 1851–1863.
[4] P.C. Wayner Jr., Y.K. Kao, L.V. Lacroix, The interline heat-transfer coefficient of an evaporating wetting film, Int. J. Heat Mass Transfer 19 (1976) 487–492.
[5] F.W. Holm, S.P. Goplen, Heat transfer in the meniscus thin-film region, J. Heat Transfer 101 (1979) 543–547.
[6] M. Sujanani, P.C. Wayner Jr., Transport processes and interfacial phenomena in an evaporating meniscus, Chem. Eng. Commun. 118 (1992) 89–110.
[7] S. Dasgupta, J.A. Schonberg, P.C. Wayner Jr., Investigation of an evaporating extended meniscus based on the augmented Young–Laplace equation, J. Heat Transfer 115 (1993) 201–208.
[8] S. Dasgupta, I.Y. Kim, P.C. Wayner Jr., Use of the Kelvin–Clapeyron equation to model an evaporating curved microfilm, J. Heat Transfer 116 (1994) 1007–1015.
[9] Q. He, K.P. Hallinan, A new particle image velocimetry technique for three-dimensional full field fluid flow measurement in evaporating films, Exp. Therm. Fluid Sci. 17 (1998) 230–237.
[10] C. Höffman, P. Stephan, Microscale temperature measurement at an evaporating liquid meniscus, Exp. Therm. Fluid Sci. 26 (2002) 157–162.
[11] S.J.S. Morris, The evaporating meniscus in a channel, J. Fluid Mech. 494 (2003) 297–317.
[12] D.A. Labunstov, Mechanism of vapor bubble growth in boiling on the heating surface, Inzhenerno-fizicheskii zhurnal 6 (4) (1963) 33–39.
[13] P. Stephan, J. Hammer, A new model for nucleate boiling heat transfer, Wärme und Stoffübertragung 30 (1994) 119–125.
[14] L.D. Koffman, M.S. Plesset, Experimental observations of the microlayer in vapor bubble growth on a heated surface, J. Heat Transfer 105 (1983) 625–632.
[15] M. Karthikeyan, J. Huang, Plawsky, P.C. Wayner Jr., Experimental study and modeling of the intermediate section of the nonisothermal constrained vapor bubble, J. Heat Transfer 120 (1998) 166–173.
[16] G. Son, V.K. Dhir, N. Ramanujapu, Dynamics and heat transfer associated with a single bubble during nucleate boiling on a horizontal surface, J. Heat Transfer 121 (1999) 623–629.
[17] G. Sateesh, S.K. Das, A.R. Balakrishnan, Analysis of pool boiling heat transfer: effect of bubbles sliding on the heating surface, Int. J. Heat Mass Transfer 48 (2004) 1543–1553.
[18] Xin Li, K. Hollingsworth, L. Witte, The thickness of the liquid microlayer between a cap-shaped sliding bubble and a heated wall: experimental measurements, J. Heat Transfer 128 (2006) 934–944.
[19] Ding Li, V.K. Dhir, Numerical study of single bubble dynamics during flow boiling, J. Heat transfer 129 (2007) 864–876.
[20] A.M. Jacobi, J.R. Thome, Heat transfer model for evaporation of elongated bubble flows in microchannels, J. Heat Transfer 124 (2002) 1131–1136.
[21] S.G. Kandlikar, Heat transfer mechanisms during flow boiling in microchannels, J. Heat Transfer 126 (2004) 8–16.
[22] J.R. Thome, Boiling in microchannels: a review of experiment and theory, Int. J. Heat Fluid Flow 25 (2005) 128–139.
[23] S.V. Patankar, Numerical Heat Transfer and Fluid Flow, Hemisphere Publishing Company, Washington, D.C., 1980.
[24] S.V. Patankar, A calculation procedure for two-dimensional elliptic situations, Numer. Heat Transfer 4 (1981) 409–425.
[25] M. Sussman, P. Smereka, S. Osher, A level set approach for computing solutions to incompressible two-phase flow, J. Comput. Phys. 114 (1994) 146–159.
[26] R.P. Fedkiw, T. Aslam, B. Merriman, S.A. Osher, Non-oscillatory Eulerian Approach to Interfaces in Multimaterial Flows (The Ghost Fluid Method) CAM Report 98-17, Department of Mathematics, UCLA, Los Angeles, 1998.
[27] A. Mukherjee, S.G. Kandlikar, Numerical simulation of growth of a vapor bubble during flow boiling of water in a microchannel, J. Microfluid. Nanofluid. 1 (2) (2005) 137–145.
[28] A. Mukherjee, Numerical and experimental study of lateral merger of vapor bubbles formed on a horizontal surface during nucleate pool boiling. Ph.D. thesis, University of California, Los Angeles, 2003.
[29] S.P. Liaw, V.K. Dhir, Void fraction measurements during saturated pool boiling of water on partially wetted vertical surfaces, J. Heat Transfer 111 (1989) 731–738.

[30] A. Mukherjee, S.G. Kandlikar, Numerical study of single bubbles with dynamic contact angle during nucleate pool boiling, Int. J. Heat Mass Transfer 50 (2007) 127–138.
[31] S. Kandlikar, Kuan Wai Keat, A. Mukherjee, Experimental study of heat transfer in an evaporating meniscus on a moving heated surface, J. Heat Transfer 127 (2005) 244–252.
[32] A. Mukherjee, S.G. Kandlikar, Numerical study of an evaporating meniscus on a moving heated surface, J. Heat Transfer 128 (12) (2006) 1285–1292.
[33] A. Mukherjee, S.G. Kandlikar, Numerical study of effect of contact angle on bubble growth and wall heat transfer during flow boiling of water in a microchannel, in: Proceedings of International Heat Transfer Conference, Sydney, Australia, 2006.